Intertwined Magnetic and Nematic Orders in Semiconducting KFe_{0.8}Ag_{1.2}Te_{2}

Yu Song, Huibo Cao, B. C. Chakoumakos, Yang Zhao, Aifeng Wang, Hechang Lei, C. Petrovic, and Robert J. Birgeneau

Intertwined magnetic and nematic orders in semiconducting $KFe_{0.8}Ag_{1.2}Te_2$

Yu Song,[1, 2, *] Huibo Cao,[3] B. C. Chakoumakos,[3] Yang Zhao,[4, 5] Aifeng Wang,[6] Hechang Lei[†, 6] C. Petrovic,[6] and Robert J. Birgeneau[1, 2, 7]

[1]*Department of Physics, University of California, Berkeley, California 94720, USA*
[2]*Materials Sciences Division, Lawrence Berkeley National Laboratory, Berkeley, California 94720, USA*
[3]*Neutron Scattering Division, Oak Ridge National Laboratory, Oak Ridge, Tennessee 37831, USA*
[4]*NIST Center for Neutron Research, National Institute of Standards and Technology, Gaithersburg, Maryland 20899, USA*
[5]*Department of Materials Science and Engineering,*
University of Maryland, College Park, Maryland 20742, USA
[6]*Condensed Matter Physics and Materials Science Department,*
Brookhaven National Laboratory, Upton, New York 11973, USA
[7]*Department of Materials Science and Engineering,*
University of California, Berkeley, California 94720, USA

Superconductivity in the iron pnictides emerges from metallic parent compounds exhibiting intertwined stripe-type magnetic order and nematic order, with itinerant electrons suggested to be essential for both. Here we use X-ray and neutron scattering to show that a similar intertwined state is realized in semiconducting $KFe_{0.8}Ag_{1.2}Te_2$ ($K_5Fe_4Ag_6Te_{10}$) without itinerant electrons. We find Fe atoms in $KFe_{0.8}Ag_{1.2}Te_2$ form isolated 2×2 blocks, separated by nonmagnetic Ag atoms. Long-range magnetic order sets in below $T_N \approx 35$ K, with magnetic moments within the 2×2 Fe blocks ordering into the stripe-type configuration. A nematic order accompanies the magnetic transition, manifest as a structural distortion that breaks the fourfold rotational symmetry of the lattice. The nematic orders in $KFe_{0.8}Ag_{1.2}Te_2$ and iron pnictide parent compounds are similar in magnitude and how they relate to the magnetic order, indicating a common origin. Since $KFe_{0.8}Ag_{1.2}Te_2$ is a semiconductor without itinerant electrons, this indicates that local-moment magnetic interactions are integral to its magnetic and nematic orders, and such interactions may play a key role in iron-based superconductivity.

PACS numbers: 74.25.Ha, 74.70.-b, 78.70.Nx

The parent compounds of the iron pnictide superconductors exhibit stripe-type magnetic order, typically accompanied or preceded by the onset of a nematic order that drives a concomitant tetragonal-to-orthorhombic structural transition [1–4]. The onset of nematic order results in the differentiation of lattice spacings along the Fe-Fe bond directions, characterized by an orthorhombicity $[\delta = (a-b)/(a+b)]$ of a few tenths of a percent. In the magnetically ordered state, spins are antiferromagnetically aligned along the longer axis and ferromagnetically aligned along the shorter axis [5, 6].

Although a multitude of different magnetic orders have been uncovered in related materials [7–23], observations of intertwined stripe-type magnetic order and nematic order are so far limited to iron pnictides such as LaFeAsO and $BaFe_2As_2$ [2, 5, 6]. Upon doping, these intertwined orders are suppressed, giving way to superconductivity near the corresponding quantum critical points [24], evidencing their intimate roles in iron-based superconductivity. The ubiquity of stripe-type magnetic [25, 26] and nematic [27] fluctuations in iron-based superconductors further reinforces this view, setting intertwined magnetic and nematic orders at the center of iron-based supercon-

ductivity research.

The stripe-type magnetic order has been suggested to originate from nesting of itinerant electrons [28, 29], or local-moments on the verge of a Mott-insulating state [30]. For the nematic order, while a ferroelastic origin has been ruled out [31, 32], the question whether it results from the magnetic or the orbital degree of freedom remains open [3]. In the magnetic scenario, nematic order results from the breaking of fourfold rotational symmetry in the spin-spin correlations of stripe-type magnetism [33–37]. In the orbital picture, the onset of nematic order is due to the lifting of orbital degeneracy [38, 39], manifest as the splitting of bands with d_{xz} and d_{yz} characters near the Fermi level [40]. In both cases, itinerant electrons near the Fermi level have been suggested to be essential for the nematic state [35, 36, 40]. Alternatively, the nematic state can result solely from local-moment stripe-type magnetism, without the need of itinerant electrons [33, 34].

In this work we reveal the presence of intertwined stripe-type magnetic order and nematic order in semiconducting $KFe_{0.8}Ag_{1.2}Te_2$ single crystals using X-ray and neutron diffraction. We find that the Fe atoms in $KFe_{0.8}Ag_{1.2}Te_2$ order into 2×2 blocks separated by nonmagnetic Ag atoms, forming a body-centered $\sqrt{5} \times \sqrt{5}$ tetragonal superstructure with the stoichiometric composition $K_5Fe_4Ag_6Te_{10}$ [Fig. 1(a) and (d)]. Below T_N,
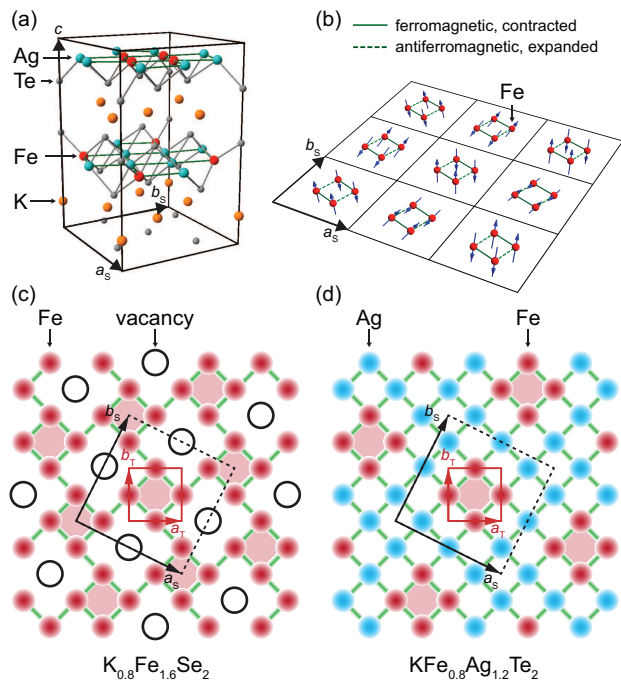
FIG. 1: (Color online) (a) Crystal structure of $KFe_{0.8}Ag_{1.2}Te_2$, with the unit cell expanded by $\sqrt{5} \times \sqrt{5}$ in the ab plane relative to the $I4/mmm$ unit cell. (b) Magnetic structure of $KFe_{0.8}Ag_{1.2}Te_2$, with only Fe atoms shown. (c) Schematic of Fe-plane in $K_{0.8}Fe_{1.6}Se_2$. (d) Schematic of Fe-Ag plane in $KFe_{0.8}Ag_{1.2}Te_2$. The solid-line boxes in (c) and (d) represent the $I4/mmm$ unit cells, and the dashed-line boxes are the $\sqrt{5} \times \sqrt{5}$ superstructure unit cells. The squares shaded in red highlight the 2×2 Fe blocks.
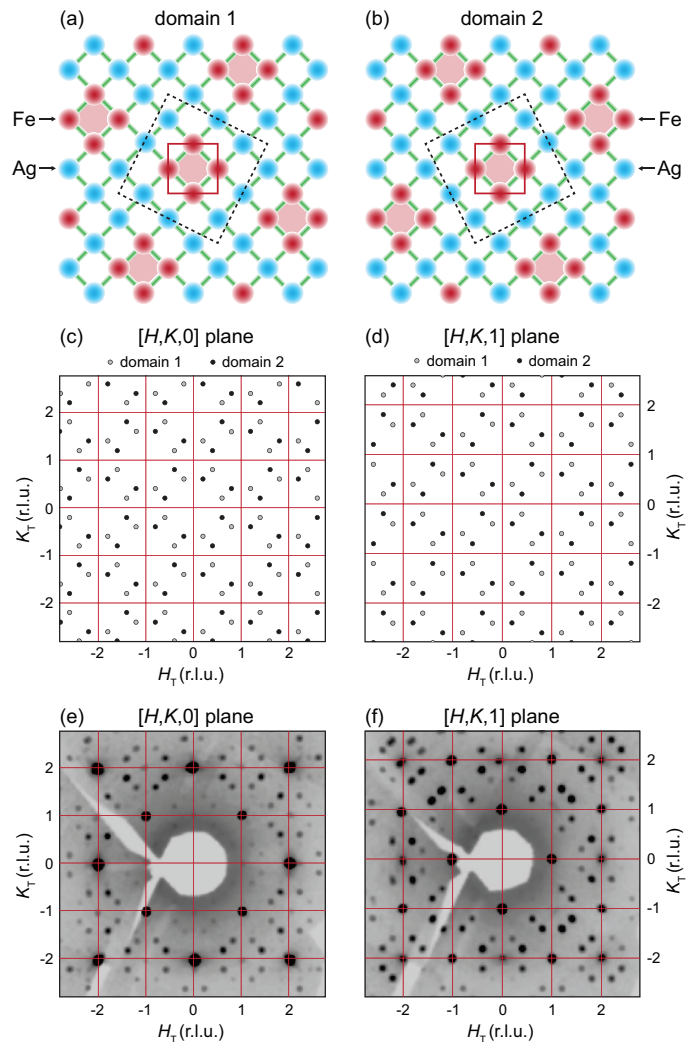

FIG. 2: (Color online) Ordering of Fe and Ag for superstructure (a) domain 1 and (b) domain 2. The presence of both domains results in superstructure peaks in reciprocal space as shown for the (c) $[H, K, 0]$ and (d) $[H, K, 1]$ planes. The superstructure peaks due to the two domains are well separated. X-ray diffraction data of $KFe_{0.8}Ag_{1.2}Te_2$ in the (e) $[H, K, 0]$ and (f) $[H, K, 1]$ scattering planes measured at 260 K. The red horizontal and vertical lines represent the reciprocal lattice of the $I4/mmm$ unit cell.

spins within each block order into a collinear stripe-type configuration, while the orientation of the spins is modulated from block to block by an incommensurate propagation vector [Fig. 1(b)]. A structural transition reflecting the onset of a nematic order accompanies the magnetic transition, breaking the fourfold rotational symmetry of the lattice. The structural transition results in an expanded lattice spacing along the Fe-Fe direction with antiferromagnetically aligned spins, and a contracted lattice spacing along the Fe-Fe direction with ferromagnetically aligned spins [Fig. 1(b)], similar to the parent compounds of the iron pnictides. In addition, the magnitude of the distortion is also similar to those in the iron pnictides, pointing to a common origin of the intertwined orders. Importantly, for $KFe_{0.8}Ag_{1.2}Te_2$ the essential physics is already present in isolated 2×2 Fe blocks, which builds up the Fe-pnictogen/chalcogen planes of iron-based superconductors. Because $KFe_{0.8}Ag_{1.2}Te_2$ is a semiconductor without itinerant electrons, its intertwined magnetic and nematic orders likely result from local-moment magnetism, with the underlying magnetic interactions also important for iron-based superconductivity.

The growth and physical properties of $KFe_{0.8}Ag_{1.2}Te_2$

single crystals have been described previously [41]. Neutron scattering measurements were carried out on the four circle diffractometer HB-3A, HFIR, Oak Ridge National Laboratory, and the BT-4 triple-axis spectrometer at the NIST Center for Neutron Research (NCNR). Single-crystal X-ray diffraction data were collected at 260 K using a Rigaku XtaLAB PRO diffractometer. Experimental details are described in the Supplemental Material [42].

Previous X-ray powder diffraction measurements suggested that $KFe_{0.8}Ag_{1.2}Te_2$ is isostructural to tetragonal $BaFe_2As_2$ (space group $I4/mmm$, $a_T = b_T \approx 4.37$ Å and
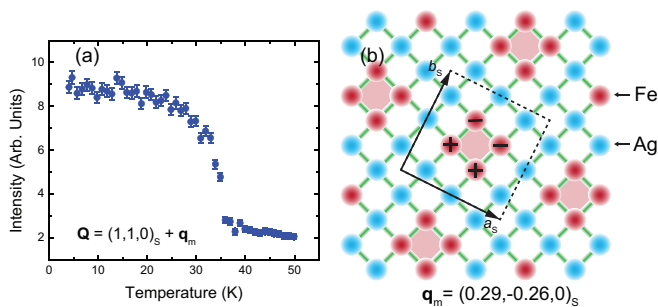
FIG. 3: (Color online) (a) Temperature dependence of magnetic intensity at $\mathbf{Q} = (1,1,0)_S + \mathbf{q}_m = (1.29, 0.74, 0)_S$. (b) Schematic of stripe-type pattern within the 2×2 block associated with $\mathbf{q}_m = (0.29, -0.26, 0)_S$. Error bars represent one standard deviation.

$c \approx 14.95$ Å), with disordered Fe and Ag [41]. Our single crystal X-ray diffraction measurements reveal a series of superstructure peaks [Figs. 2(c)-(f)] that indicate a unit cell expanded by $\sqrt{5} \times \sqrt{5}$ in the ab plane due to the ordering of Fe and Ag, forming two structural domains that are mirror images of each other [Figs. 2(a), (b)], similar to iron-vacancy-ordered $K_{0.8}Fe_{1.6}Se_2$ ($K_2Fe_4Se_5$) [Figs. 1(c), (d)] [11]. Reciprocal lattice vectors for the two superstructure domains can be obtained from that of the $I4/mmm$ unit cell in reciprocal lattice units (r. l. u.), using $H_S = 2H_T - K_T$, $K_S = H_T + 2K_T$ (the subscripts are used to distinguish vectors in different notations) for one structural domain [Fig. 2(a)], and $H_S = 2H_T + K_T$, $K_S = -H_T + 2K_T$ for the other [Fig. 2(b)]. The crystal structure of $KFe_{0.8}Ag_{1.2}Te_2$ is body-centered and exhibits four-fold rotational symmetry with space group $I4$, detailed in Table I. Bragg peaks associated with the superstructure are well separated in reciprocal space for the two structural domains, allowing them to be easily distinguished [Figs. 2(c), (d)].

To elucidate the magnetic structure of $KFe_{0.8}Ag_{1.2}Te_2$, we systematically studied magnetic Bragg peaks exclusively associated with one of the superstructural domains [Fig. 2(a)] using HB-3A. We found that magnetic Bragg peaks occur at $\mathbf{Q} = \boldsymbol{\tau}_S \pm \mathbf{q}_m$, where $\boldsymbol{\tau}_S$ are structural Bragg peaks of the $\sqrt{5} \times \sqrt{5}$ unit cell, and $\mathbf{q}_m = (0.29(1), -0.26(1), 0)_S$ is the incommensurate magnetic propagation vector, suggesting that the magnetic structure does not exhibit four-fold rotational symmetry. Measurement of the magnetic intensity which scales like the magnetic order parameter squared, is shown in Fig. 3(a) for $\mathbf{Q} = (1,1,0)_S + \mathbf{q}_m$, revealing a clear onset of magnetic order below $T_N \approx 35$ K, in good agreement with susceptibility measurements [41].

We find the magnetic moments inside each Fe block form a collinear stripe-type pattern with an ordered moment of $2.11(3)$ μ_B/Fe, as shown in Fig. 1(b) and Fig. 3(b). The spin orientations of the 2×2 blocks are modulated from block to block by $\mathbf{q}_m$, resulting from the weak

spin anisotropy as indicated in susceptibility measurements [41], and the presence of small inter-block couplings. The magnetic unit cell of $KFe_{0.8}Ag_{1.2}Te_2$ contains a single 2×2 Fe block with 4 Fe atoms. This means that, compared to the magnetic structure of the iron pnictides which contains a single Fe atom, a magnetic structure factor $|F(\mathbf{Q})|^2 = |\sum_{j=1}^{4} \mathbf{m}_j \exp(-i\mathbf{Q} \cdot \mathbf{r}_j)|^2$ modulates the intensities of the magnetic Bragg peaks that occur at $\mathbf{Q} = \boldsymbol{\tau}_S \pm \mathbf{q}_m$, and such a modulation provides direct evidence for the stripe-type configuration within the Fe blocks. While magnetic Bragg peaks in $KFe_{0.8}Ag_{1.2}Te_2$ occur at an incommensurate propagation vector associated with the $\sqrt{5} \times \sqrt{5}$ unit cell rather than the stripe vector $\mathbf{Q} = (0.5, 0.5)_T$ in iron pnictides, the magnetic structure factor $|F(\mathbf{Q})|^2$ that modulates the intensities of the magnetic Bragg peaks is peaked at $\mathbf{Q} = (0.5, 0.5)_T$ positions, due to the stripe-type pattern within the Fe blocks (See Supplemental Material for details [42]).

Since the magnetic structure breaks fourfold rotational symmetry of the paramagnetic tetragonal lattice, it is important to clarify if a nematic order breaking the same symmetry is also present and how it relates to the nematic order in the iron pnictides. In single crystals of the iron pnictides such as $BaFe_2As_2$ [43], four orthorhombic domains form below the tetragonal-to-orthorhombic structural transition temperature [Figs. 4(a) and (c)], resulting in the splitting of $(2,2,0)_T$ and $(2,0,0)_T$ peaks. $(2,2,0)_T$ splits into a quartet [Figs. 4(b) and (d)], with the separation of the peaks along the longitudinal and the transverse directions dQ related to the orthorhombicity δ through $dQ \approx 2\delta|\mathbf{Q}|$. While $(2,0,0)_T$ also splits into four peaks, the splitting is mostly along the transverse direction with two peaks overlapping in the center straddled by the other two peaks on each side [Figs. 4(b) and (d)]; the separation between the two peaks on the sides is $dQ \approx 4\delta|\mathbf{Q}|$.

Using BT-4 we carried out longitudinal and transverse scans at $\mathbf{Q} = (2,2,0)_T$ and $\mathbf{Q} = (2,0,0)_T$ below and above T_N in $KFe_{0.8}Ag_{1.2}Te_2$, to see if a similar distortion occurs. Clear broadening from 40 K to 6 K can be seen in the longitudinal and transverse scans at $(2,2,0)_T$ and the transverse scan at $(2,0,0)_T$, while a much smaller or no broadening is seen for the longitudinal scan at $(2,0,0)_T$ [insets in Figs. 4(e)-(h)]. Using scans well above T_N ($T = 70$ K) as peak line-shapes, we fitted longitudinal and transverse scans at $(2,2,0)_T$ and longitudinal scans at $(2,0,0)_T$ at different temperatures using two split peaks separated by dQ, and transverse scans at $(2,0,0)_T$ using three peaks with the two side peaks separated by dQ. The fit results, after dividing by the corresponding $|\mathbf{Q}|$, are shown in Figs. 4(e)-(h). For $(2,2,0)_T$, the splittings are similar along the longitudinal and transverse directions, whereas for $(2,0,0)_T$ the splitting occurs predominantly along the transverse direction, demonstrating that the structural distortion is dominated by differ-

TABLE I: Refined structural parameters for $KFe_{0.8}Ag_{1.2}Te_2$ from X-ray diffraction data measured at 260 K. Space group is $I4$ with $a = b = 9.7857(7)$ Å and $c = 14.933(3)$ Å.

Atom	Site	x	y	z	Occupancy	U_{eq} (Å^2)
K	$2a$	1/2	1/2	0.6472(9)	1	0.043(2)
K	$8c$	0.5978(4)	0.8044(4)	0.1680(7)	1	0.0427(12)
Fe	$8c$	0.39925(18)	0.69461(18)	0.9123(4)	1	0.0196(4)
Ag	$4b$	1/2	0	0.91705(16)	1	0.0324(6)
Ag	$8c$	0.08740(16)	0.79877(12)	0.91032(16)	1	0.0335(5)
Te	$2a$	0	0	0.7851(2)	1	0.0355(9)
Te	$2a$	1/2	1/2	0.01838(18)	1	0.0281(6)
Te	$8c$	0.30304(10)	0.87686(17)	0.02736(10)	1	0.0333(4)
Te	$8c$	0.59148(10)	0.78865(11)	0.79997(8)	1	0.0316(4)

ing lattice spacings along the Fe-Fe bond directions, similar to iron pnictides such as $BaFe_2As_2$. Coupled with the $\sqrt{5} \times \sqrt{5}$ superstructure in $KFe_{0.8}Ag_{1.2}Te_2$, the crystal system would become monoclinic or triclinic since the angle between a_S and b_S is no longer 90°; nonetheless, the main effect of the structural distortion is the differentiation of lattice spacings along the Fe-Fe direction that can be characterized by a similar orthorhombicity as defined for iron pnictides. For longitudinal and transverse scans at $(2,2,0)_T$, $dQ/|\mathbf{Q}| \approx 2\delta$; for the transverse scan at $(2,0,0)_T$, $dQ/|\mathbf{Q}| \approx 4\delta$. The values of δ obtained from Figs. 4(e)-(g) are consistent and average to $\delta \approx 3.8 \times 10^{-3}$, which is close to $\delta \approx 4.0 \times 10^{-3}$ for $BaFe_2As_2$ [6]. Moreover, we find that the expanded lattice spacing is associated with the antiferromagnetically aligned Fe-Fe bond direction, whereas the contracted lattice spacing is associated with the ferromagnetically aligned Fe-Fe bond direction (See Supplemental Material for details [42]), which is the same as in the iron pnictide parent compounds.

Our observation of intertwined stripe-type magnetic order and nematic order in $KFe_{0.8}Ag_{1.2}Te_2$ is different from observations of stripe-type magnetism in $KFe_{1.5}Se_2$ ($K_2Fe_3Se_4$) [15] and heavily Cu-doped $NaFe_{1-x}Cu_xAs$ [22] and $Ba(Fe_{1-x}Cu_x)_2As_2$ [23]. In the latter cases, there are no nematic orders that accompany the onset of magnetic orders. Since $KFe_{0.8}Ag_{1.2}Te_2$ is a semiconductor without itinerant electrons near the Fermi level [41, 44], it provides an experimental benchmark to identify whether properties related the intertwined orders require contributions from itinerant electrons; properties intrinsic to the intertwined orders should be present in both iron pnictides and $KFe_{0.8}Ag_{1.2}Te_2$, whereas properties that require itinerant electrons would be present in iron pnictides but not in $KFe_{0.8}Ag_{1.2}Te_2$. The semiconducting nature of $KFe_{0.8}Ag_{1.2}Te_2$ further suggests local-moment magnetic interactions are responsible for its intertwined orders, different from the itinerant-electron scenarios proposed for the iron pnictides [35, 36]. Given the multi-orbital nature of Fe, orbital physics could also

play an important role, although its manifestation in $KFe_{0.8}Ag_{1.2}Te_2$ would be quite different from that in the iron pnictides that exhibit split bands of d_{xz} and d_{yz} characters near the Fermi level [40]. We note that $T_N \approx 35$ K in $KFe_{0.8}Ag_{1.2}Te_2$ is considerably lower than $T_N > 500$ K in $K_{0.8}Fe_{1.6}Se_2$, most likely due to weak inter-block couplings that bottleneck the formation of long-range magnetic order. We expect that intra-block interactions should exhibit a much larger energy scale, with magnetic fluctuations that extend to high energies present around both $\mathbf{Q} = (0.5, 0.5)_T$ and $\mathbf{Q} = (0.5, -0.5)_T$ in the paramagnetic state well above T_N. The intertwined magnetic and nematic orders imply the presence of intense fluctuations of both, near the quantum critical point where the intertwined orders are suppressed. Given that superconductivity typically arises in the neighborhood of such putative quantum critical points in the iron pnictides [24], suppressing the intertwined orders in $KFe_{0.8}Ag_{1.2}Te_2$ through doping or the application of pressure may lead to a novel superconducting state.

Our results also highlight the use of nonmagnetic elements to tune the physical properties of systems containing Fe-pnictogen/chalcogen planes, similar to iron-vacancy tuning in $K_zFe_{2-y}Se_2$ [11, 15]. Such tuning has been explored in $A(Fe_{1-x}B_x)_2Ch_2$ (A = K, Na, Rb; B = Li, Cu, Ag; Ch = S, Se, Te) with $x \approx 50\%$ [45, 46], and most such systems appear to exhibit a spin-glass ground state. Our crystal refinement results indicate that the ideal ratio of Fe and Ag is 2:3 in $KFe_{0.8}Ag_{1.2}Te_2$, this may explain why $KFe_{1.05}Ag_{0.88}Te_2$ exhibits a spin-glass ground state without long-range magnetic order [47, 48]. Similarly, the prevalence of a spin-glass ground state in $A(Fe_{1-x}B_x)_2Ch_2$ [45] may be due to most reported compounds being close to a 1:1 ratio of Fe and the nonmagnetic B element, rather than a ratio close to 2:3 as in $KFe_{0.8}Ag_{1.2}Te_2$. The availability of numerous similar systems [45] presents a unique opportunity to investigate the effects of magnetic dilution and chemical pressure on the physical properties of Fe-pnictogen/chalcogen planes,
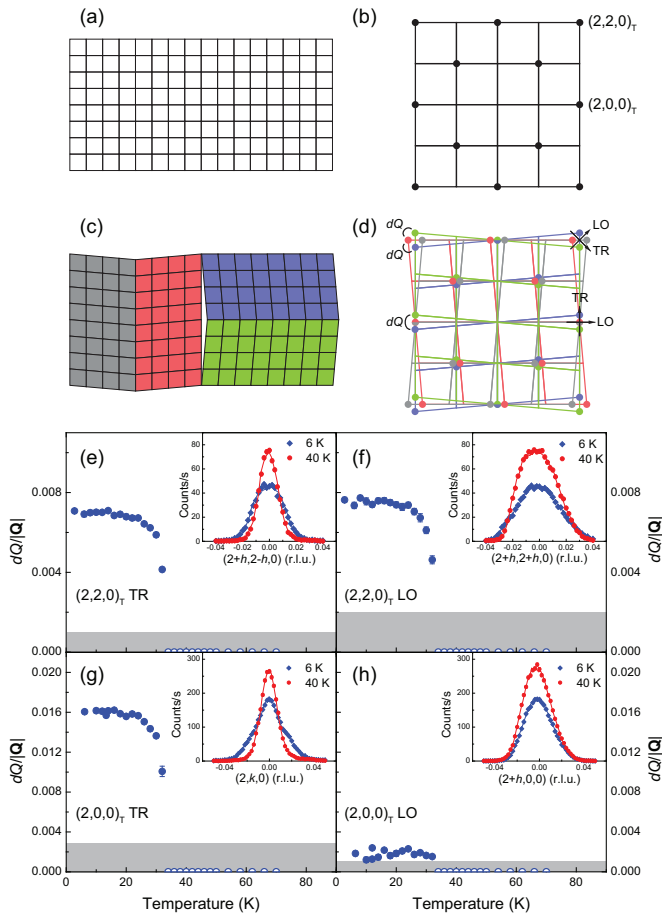
FIG. 4: (Color online) Schematic of the (a) real and (b) reciprocal space lattices of $BaFe_2As_2$ in the tetragonal phase. Upon cooling below the tetragonal-to-orthorhombic transition temperature, four structural domains as shown in (c) form in $BaFe_2As_2$, resulting in splitting of Bragg peaks in reciprocal space shown in (d). (a)-(d) are adapted from Ref. [43]. $dQ/|\mathbf{Q}|$ for $KFe_{0.8}Ag_{1.2}Te_2$ for (e) transverse and (f) longitudinal scans at $(2,2,0)_T$. Similarly, for (g) transverse and (h) longitudinal scans at $(2,0,0)_T$. For $T \geq 35$ K, we do not observe broadening within our resolution (shaded gray area), therefore for these points $dQ/|\mathbf{Q}|$ are set to be zero (open symbols). The insets in (e)-(h) compare corresponding scans at 6 K and 40 K, the solid lines are fits to the data as described in the text. Error bars represent one standard deviation.

by tuning the ratio of Fe and the nonmagnetic B element, and by replacing Ag with other nonmagnetic elements or Te with other chalcogens.

In summary, we find that Fe atoms in $KFe_{0.8}Ag_{1.2}Te_2$ order into isolated 2×2 blocks, forming a $\sqrt{5} \times \sqrt{5}$ superstructure. Below $T_N \approx 35$ K, magnetic moments within the Fe blocks form a stripe-type pattern accompanied by a nematic order that breaks fourfold rotational symmetry of the crystal structure, exhibiting a phenomenology similar to the iron pnictides. Since $KFe_{0.8}Ag_{1.2}Te_2$ is a semiconductor, these intertwined orders should be driven by local-moment magnetism originating from the

minimal quartet of 4 Fe spins, and the underlying interactions should be important for the physics of materials with Fe-pnictogen/chalcogen planes in general, including iron-based superconductors.

* Electronic address: yusong@berkeley.edu
[1] G. R. Stewart, Rev. Mod. Phys. **83**, 1589 (2011).
[2] Pengcheng Dai, Rev. Mod. Phys. **87**, 855 (2015).
[3] R. M. Fernandes, A. V. Chubukov, and J. Schmalian, Nat. Phys. **10**, 97-104 (2014).
[4] Qimiao Si, Rong Yu, and Elihu Abrahams, Nat. Rev. Mater. **1**, 16017 (2016).
[5] Clarina de la Cruz, Q. Huang, J. W. Lynn, Jiying Li, W. Ratcliff II, J. L. Zarestky, H. A. Mook, G. F. Chen, J. L. Luo, N. L. Wang, and Pengcheng Dai, Nature **453**, 899-902 (2008).
[6] Q. Huang, Y. Qiu, Wei Bao, M. A. Green, J. W. Lynn, Y. C. Gasparovic, T. Wu, G. Wu, and X. H. Chen, Phys. Rev. Lett. **101**, 257003 (2008).
[7] Wei Bao, Y. Qiu, Q. Huang, M. A. Green, P. Zajdel, M. R. Fitzsimmons, M. Zhernenkov, S. Chang, Minghu Fang, B. Qian, E. K. Vehstedt, Jinhu Yang, H. M. Pham, L. Spinu, and Z. Q. Mao, Phys. Rev. Lett. **102**, 247001 (2009).
[8] Yogesh Singh, M. A. Green, Q. Huang, A. Kreyssig, R. J. McQueeney, D. C. Johnston, and A. I. Goldman, Phys. Rev. B **80**, 100403 (2009).
[9] D. G. Quirinale, V. K. Anand, M. G. Kim, Abhishek Pandey, A. Huq, P. W. Stephens, T. W. Heitmann, A. Kreyssig, R. J. McQueeney, D. C. Johnston, and A. I. Goldman, Phys. Rev. B **88**, 174420 (2013).
[10] Xiaoyan Tan, Gilberto Fabbris, Daniel Haskel, Alexander A. Yaroslavtsev, Huibo Cao, Corey M. Thompson, Kirill Kovnir, Alexey P. Menushenkov, Roman V. Chernikov, V. Ovidiu Garlea, and Michael Shatruk, J. Am. Chem. Soc. **138**, 2724 (2016).
[11] Wei Bao, Qing-Zhen Huang, Gen-fu Chen, M. A. Green, Du-Ming Wang, Jun-Bao He, Yi-Ming Qiu, Chin. Phys. Lett. **28**, 086104 (2011).
[12] F. Ye, S. Chi, Wei Bao, X. F. Wang, J. J. Ying, X. H. Chen, H. D. Wang, C. H. Dong, and Minghu Fang, Phys. Rev. Lett. **107**, 137003 (2011).
[13] Meng Wang, Miaoyin Wang, G. N. Li, Q. Huang, C. H. Li, G. T. Tan, C. L. Zhang, Huibo Cao, Wei Tian, Yang Zhao, Y. C. Chen, X. Y. Lu, Bin Sheng, H. Q. Luo, S.

L. Li, M. H. Fang, J. L. Zarestky, W. Ratcliff, M. D. Lumsden, J. W. Lynn, and Pengcheng Dai, Phys. Rev. B **84**, 094504 (2011).

[14] Brian C. Sales, Michael A. McGuire, Andrew F. May, Huibo Cao, Bryan C. Chakoumakos, and Athena S. Sefat, Phys. Rev. B **83**, 224510 (2011).

[15] Jun Zhao, Huibo Cao, E. Bourret-Courchesne, D.-H. Lee, and R. J. Birgeneau, Phys. Rev. Lett. **109**, 267003 (2012).

[16] Huibo Cao, Claudia Cantoni, Andrew F. May, Michael A. McGuire, Bryan C. Chakoumakos, Stephen J. Pennycook, Radu Custelcean, Athena S. Sefat, and Brian C. Sales, Phys. Rev. B **85**, 054515 (2012).

[17] Andrew F. May, Michael A. McGuire, Huibo Cao, Ilya Sergueev, Claudia Cantoni, Bryan C. Chakoumakos, David S. Parker, and Brian C. Sales, Phys. Rev. Lett. **109**, 077003 (2012).

[18] Meng Wang, Ming Yi, Huibo Cao, C. de la Cruz, S. K. Mo, Q. Z. Huang, E. Bourret-Courchesne, Pengcheng Dai, D. H. Lee, Z. X. Shen, and R. J. Birgeneau, Phys. Rev. B **92**, 121101(R) (2015).

[19] K. M. Taddei, M. Sturza, D. Y. Chung, H. B. Cao, H. Claus, M. G. Kanatzidis, R. Osborn, S. Rosenkranz, and O. Chmaissem, Phys. Rev. B **92**, 094505 (2015).

[20] J. M. Caron, J. R. Neilson, D. C. Miller, A. Llobet, and T. M. McQueen, Phys. Rev. B **84**, 180409 (2011).

[21] Fei Du, Kenya Ohgushi, Yusuke Nambu, Takateru Kawakami, Maxim Avdeev, Yasuyuki Hirata, Yoshitaka Watanabe, Taku J Sato, and Yutaka Ueda, Phys. Rev. B **85**, 214436 (2012).

[22] Yu Song, Zahra Yamani, Chongde Cao, Yu Li , Chenglin Zhang, Justin S. Chen, Qingzhen Huang, Hui Wu, Jing Tao, Yimei Zhu, Wei Tian, Songxue Chi, Huibo Cao, Yao-Bo Huang, Marcus Dantz, Thorsten Schmitt, Rong Yu, Andriy H. Nevidomskyy, Emilia Morosan, Qimiao Si, and Pengcheng Dai, Nat. Commun. **7**, 13879 (2016).

[23] Weiyi Wang, Yu Song, Ding Hu, Yu Li, Rui Zhang, L. W. Harriger, Wei Tian, Huibo Cao, and Pengcheng Dai, Phys. Rev. B **96**, 161106 (2017).

[24] T. Shibauchi, A. Carrington, and Y. Matsuda, Annu. Rev. Condens. Matter Phys. **5**, 113-135 (2014).

[25] A. D. Christianson, E. A. Goremychkin, R. Osborn, S. Rosenkranz, M. D. Lumsden, C. D. Malliakas, I. S. Todorov, H. Claus, D. Y. Chung, M. G. Kanatzidis, R. I. Bewley, and T. Guidi, Nature **456** 930-932 (2008).

[26] Qisi Wang, Yao Shen, Bingying Pan, Yiqing Hao, Mingwei Ma, Fang Zhou, P. Steffens, K. Schmalzl, T. R. Forrest, M. Abdel-Hafiez, Xiaojia Chen, D. A. Chareev, A. N. Vasiliev, P. Bourges, Y. Sidis, Huibo Cao, and Jun Zhao, Nat. Mater. **15**, 159-163 (2016).

[27] Hsueh-Hui Kuo, Jiun-Haw Chu, Johanna C. Palmstrom, Steven A. Kivelson, and Ian R. Fisher, Science **352**, 958-962 (2016).

[28] I. I. Mazin, Nature **464**, 183-186 (2010).

[29] P. J. Hirschfeld, M. M. Korshunov, and I. I. Mazin, Rep. Prog. Phys. **74**, 124508 (2011).

[30] Qimiao Si, and Elihu Abrahams, Phys. Rev. Lett. **101**, 076401 (2008).

[31] Jiun-Haw Chu, James G. Analytis, Kristiaan De Greve, Peter L. McMahon, Zahirul Islam, Yoshihisa Yamamoto,

and Ian R. Fisher, Science **329**, 824-826 (2010).

[32] Jiun-Haw Chu, Hsueh-Hui Kuo, James G. Analytis, and Ian R. Fisher, Science **337**, 710-712 (2012).

[33] Chen Fang, Hong Yao, Wei-Feng Tsai, JiangPing Hu, and Steven A. Kivelson, Phys. Rev. B **77**, 224509 (2008).

[34] Cenke Xu, Markus Müller, and Subir Sachdev, Phys. Rev. B **78**, 020501 (2008).

[35] R. M. Fernandes, A. V. Chubukov, J. Knolle, I. Eremin, and J. Schmalian, Phys. Rev. B **85**, 024534 (2012).

[36] Rafael M. Fernandes, and Jörg Schmalian, Supercond. Sci. Technol. **25**, 084005 (2012).

[37] S. Liang, A. Moreo, and E. Dagotto, Phys. Rev. Lett. **111**, 047004 (2013).

[38] Weicheng Lv, Jiansheng Wu, and Philip Phillips, Phys. Rev. B **80**, 224506 (2009).

[39] Chi-Cheng Lee, Wei-Guo Yin, and Wei Ku, Phys. Rev. Lett. **103**, 267001 (2009).

[40] Ming Yi, Donghui Lu, Jiun-Haw Chu, James G. Analytis, Adam P. Sorini, Alexander F. Kemper, Brian Moritz, Sung-Kwan Mo, Rob G. Moore, Makoto Hashimoto, Wei-Sheng Lee, Zahid Hussain, Thomas P. Devereaux, Ian R. Fisher, and Zhi-Xun Shen, Proc. Natl. Acad. Sci. U.S.A. **108**, 6878 (2011).

[41] Hechang Lei, Emil S. Bozin, Kefeng Wang, and C. Petrovic, Phys. Rev. B **84**, 060506(R) (2011).

[42] See Supplemental Material for experimental details, determination of the magnetic structure and how the structural distortion relates to the magnetic order, which includes Refs. [49–53].

[43] M. A. Tanatar, A. Kreyssig, S. Nandi, N. Ni, S. L. Bud'ko, P. C. Canfield, A. I. Goldman, and R. Prozorov, PHys. Rev. B **79**, 180508 (2009).

[44] R. Ang, K. Nakayama, W.-G. Yin, T. Sato, Hechang Lei, C. Petrovic, and T. Takahashi, Phys. Rev. B **88**, 155102 (2013).

[45] Duanduan Yuan, Ning Liu, Kunkun Li, Shifeng Jin, Jiangang Guo, and Xiaolong Chen, Inorg. Chem. **56**, 13187-13193 (2017).

[46] Fan Sun, Zhongnan Guo, Ning Liu, Kun Lin, Da Wang, and Wenxia Yuan, Dalton Trans. **46**, 3649 (2017).

[47] Hyejin Ryu, Hechang Lei, B. Klobes, J. B. Warren, R. P. Hermann, and C. Petrovic, Phys. Rev. B **91**, 174517 (2015).

[48] We note the spin-glass behavior in $KFe_{1.05}Ag_{0.88}Te_2$ may be due to disorder acting as a random field that pins the nematic order, resulting in a random-field nematic-glass. Due to the intertwined nature of the nematic and magnetic orders, the spin-glass behavior then follows from the nematic-glass in this scenario.

[49] Rigaku, CrystalClear. Rigaku Corporation, Tokyo, Japan (2005).

[50] G. M. Sheldrick, Acta Crystallogr. **A64**, 112-122 (2008).

[51] L. J. Farrugia, J. Appl. Cryst. **45**, 849-854 (2012).

[52] B. C. Chakoumakos, H. B. Cao, F.Ye, A.D. Stoica, M. Popovici, M. Sundaram, W. Zhou, J. S. Hicks, G. W. Lynn, and R. A. Riedel, J. Appl. Crystallogr. **44**, 655 (2011).

[53] J. Rodriguez-Carvajal, Physica B **192**, 55 (1993).